COMMUNICATIONS IN SCIENCE AND TECHNOLOGY
Homepage: cst.kipmi.or.id

Synthesis of Cu nanoparticles using *Anredera cordifolia* extract and their potential as antidiabetic with alpha amylase enzyme inhibition

Nurharis Munandar*, Henry F. Aritonang, Ridho Bonaventura, Dwi Putra Wijaya

Department of Chemistry, Universitas Sam Ratulangi, Manado 95115, Indonesia

Article history:
Received: 26 October 2025 / Received in revised form: 19 December 2025 / Accepted: 21 December 2025

Abstract

This study reports a green synthesis of copper nanoparticle using binahong (*Anredera cordifolia*) leaf extract as both a bioreductant and a capping agent. The synthesis was optimized by varying the extract-to-precursor ratio (1:3, v/v) and the reaction pH (6–11) with pH 10 selected as the optimal condition for nanoparticle preparation. Nanoparticle formation was confirmed using UV–Vis spectroscopy, showing a strong absorption band at 325 nm, indicative of oxide-based copper nanostructures and/or surface oxidation during green synthesis. XRD patterns revealed Cu_2O as the dominant crystalline phase, characterized by reflections at $2\theta \approx 29.6°$, 36.4°, 42.3°, 61.3°, 73.5°, and 77.3°, with a possible minor contribution from metallic Cu due to peak overlap. FTIR spectra confirmed the presence of biomolecules (O–H and C–H bands, along with carbonyl/COO^--related bands) involved in nanoparticle stabilization, as well as Cu–O vibrations around 600–620 cm^{-1} consistent with Cu_2O. PSA showed a dominant hydrodynamic size in the 60–70 nm range (average 65 nm), whereas SEM indicated aggregation into micrometer-scale clusters upon drying. In vitro α-amylase inhibition assays demonstrated concentration-dependent inhibition, with CuNPs (IC_{50} 6.18 µg/mL) and the extract + CuNPs mixture (IC_{50} 6.83 µg/mL) approaching that of acarbose (IC_{50} 5.04 µg/mL) and exhibiting stronger activity than the extract alone (IC_{50} 8.89 µg/mL). The key contribution of this work is the development of a simple, aqueous, environmentally friendly route that leverages local biological resources while producing Cu_2O-rich nanoparticles with α-amylase inhibitory activity approaching that of acarbose. These findings highlight the promise of a low-cost antidiabetic candidate for postprandial glucose control and provide a basis for further investigations into nanoformulation and preclinical evaluation.

Keywords: Copper nanoparticles; binahong extract; green synthesis; α-amylase inhibition; antidiabetic

1. Introduction

Diabetes mellitus (DM) is a metabolic disorder resulting from the inability of the pancreas to impair insulin secretion or the body's resistance to insulin, causing elevated blood glucose levels [1]. In 2019, approximately 463 million people aged 20-79 years had diabetes, and with projections reaching 700 million by 2045 [2]. DM is becoming global health challenge due to the increasing number of patients and complications that damage blood vessels, increasing morbidity and mortality [3,4].

One of the key molecular mechanisms underlying DM-related complications is oxidative stress. It results from an increase in free radicals or a decrease in antioxidant activity. Unstable free radicals can damage lipids, proteins and nucleic acids, contributing to various diseases. In DM, redox imbalance increases the production of superoxide (O^{2-}), which reacts to generate peroxynitrite ($OONO^-$), exacerbating oxidative stress and endothelial dysfunction [5].

* Corresponding author.
Email: harismunandar@unsrat.ac.id
https://doi.org/10.21924/cst.10.2.2025.1829

Antioxidant administration scavenges reactive oxygen species and prevents vascular complications. Supplements that increase NO bioavailability can improve endothelial and mitochondrial function and suppress NAD(P)H oxidase activity. Endogenous antioxidants such as superoxide dismutase and glutathione, as well as synthetic ones, can control blood glucose levels and prevent complications [6]. However, synthetic drugs often cause side effects, such as adverse effects and gastrointestinal disturbances, so safer alternative agents are needed.

Metal ions such as vanadium, zinc, manganese, copper, and chromium have been reported to exhibit antidiabetic activity [7]. Inhibition of α-glucosidase and α-amylase enzymes is known to suppress postprandial hyperglycemia, but studies on metal nanoparticles as antidiabetic agents remain limited [8]. Roseline and Priya [9] reported that copper nanoparticles synthesized via biological method more effectively inhibited α-glucosidase and α-amylase than acarbose. Ghosh et al. [10] reported that copper nanoparticles (CuNPs) synthesized with *Dioscorea bulbifera* extract exhibited stronger inhibitory activity against α-glucosidase and α-amylase than acarbose.

As a transition metal, copper plays an important role in

biochemical pathways including oxygen transfer and redox-related catalytic activity. CuNPs are considered relatively biocompatible than other metal nanoparticles, so they have wider therapeutic potential [11]. CuNPs also have high stability, are cost-effective, and are widely used in catalysts, sensors, antimicrobial agents, and antioxidants [12]. Plant-based CuNP synthesis is an efficient strategy with potential to modulate hyperglycemia because copper is known to inhibit α-amylase. Binahong (*Anredera cordifolia*) was chosen because it has antidiabetic, antimicrobial, antihyperlipidemic activity, antitumor, and anti-inflammatory activities [13]. Bioactive compounds such as flavonoids and tannins act as antioxidants and antidiabetics [10]. Based on research conducted by Munandar et al. [14], copper nanoparticles and Binahong leaf extract used as a bioreductor had antioxidant activity of 34.20 µg/mL and 31.03 µg/mL, so copper nanoparticles synthesized using Binahong leaf extract have potential as antidiabetics. Those studies also showed the results of the phytochemical test of Binahong leaf extract showing the content of secondary metabolite compounds, namely flavonoids, saponins, and tannins. Based on this background, the aim of this study is to analyze the synthesis of CuNPs using Binahong and evaluate their antidiabetic properties. Furthermore, studies on α-amylase inhibition by CuNPs are still limited.

2. Materials and Methods

This study utilized a number of laboratory instruments to support the testing of alpha-amylase enzyme inhibitory activity as an indicator of antidiabetic potential. Details of the materials used as well as the methodological procedures are described in the following sections.

2.1. Chemicals and Instrumentation

The materials used included Binahong (*Anredera cordifolia*) leaf samples, Copper (II) nitrate trihydrate ($Cu(NO_3)_2{\cdot}3H_2O$) obtained from Sigma-Aldrich and used without further purification. Deionized water was used in all experimental steps for making molar solutions, washing, and dilution. In addition, $FeCl_3$ 1 M (Merck), $Pb(CH_3COO)_2$ 0.5 M (Merck), H_2SO_4 5 M (Merck), acetic anhydride 1 M (Merck), $CHCl_3$ 1 M (Merck), HCl 1% (Merck), Dragendorff's reagent, Mayer reagent, Whatman No. 42 filter paper, α-amylase enzyme (EC3.2.1.1) (Sigma-Aldrich, A8220), maltose monohydrate dissolved in distilled water, phosphate buffer (pH 7) 50 mM, 3,5-dinitro salicylic acid (DNS) reagent 1% (W/V), dimethyl sulfoxide (DMSO) 0.5% (V/V), acarbose (glucobay) (Sigma-Aldrich, A8980) and ice cubes.

Meanwhile, the instruments and equipment used included pyrex glassware, Velp Scientifica stirrer, DraonLab micropipette, Gallenhamp angle head centrifuge, Ohaus AP-110 analytical balance, pH meter (Hanna Instruments), Thermo Scientific Vortex Mixer, DLAB Incubator DHP Series, Memmert UN30 oven, BM100 water bath, Velp Scientifica multistirrer, Shimadzu UV-2600 UV-Vis spectrophotometer, Shimadzu Prestige-21 FTIR spectroscopy, Shimadzu 7000 X-ray Diffraction Instrument, Beckman Coulter Delsa Nano C Particle Size Analysis, and SEM (Scanning Electron Microscopy) JEOL JSM-IT500.

2.2. Preparation of the plant extract

The sample used was Binahong (*Anredera cordifolia*) leaf. The sample was dried and ground until smooth, then weighed as much as 5 grams. Next, the sample was boiled to a boil using 100 mL of aquabides and allowed to cool and filtered with Whatmann No. 42 filter paper.

2.3. Phytochemical analysis

Qualitative phytochemical screening of secondary metabolites of Binahong leaf water extract included tannin tests using $FeCl_3$ reagent, flavonoid test using lead acetate and sulfuric acid, saponin test with frothing test, steroid test using acetic anhydride and sulfuric acid, terpenoid test using chloroform and concentrated sulfuric acid, and alkaloid tests using Dragendorff's and Mayer's reagents.

2.4. Determination of Optimum pH

The synthesis was carried out using an optimal extract precursor ratio of 1:3 [14], and followed by pH adjustment to 6, 7, 8, 9, 10, and 11. The adjustment of pH was performed by dropwise addition of 0.1 M NaOH while stirring with a magnetic stirrer. The resulting solution was then analyzed using UV-Vis spectrophotometry to determine the maximum absorption wavelength (λmax) and determine the optimal pH for CuNP synthesis.

2.5. Cu nanoparticles synthesis procedure

Binahong extract solution and 0.01 M $Cu(NO_3)_2.3H_2O$ solution were mixed at an extract-to-precursor volume ratio of 1:3 (v/v) and the pH was adjusted to 10. The mixture was stirred at room temperature for 2 hours using a magnetic stirrer at a speed of 3000 rpm. The mixture was then allowed to stand for 24 hours, where there was a change in color and the formation of copper nanoparticle precipitates was observed. Next, the mixture was centrifuged at 10000 rpm for 30 minutes. The precipitate was washed repeatedly (2–3 times) with deionized water. The copper nanoparticle precipitate was dried using a freeze dryer.

2.6. Characterization of synthesized Cu nanoparticles

The synthesized copper nanoparticles were characterized using several instrumental techniques, namely UV-Vis Spectrophotometry, Fourier Transform Infrared Spectroscopy (FT-IR), X-ray Diffraction (XRD), Scanning Electron Microscopy (SEM), and Particle Size Analyzer (PSA). UV-Vis spectrophotometry was used to confirm the formation of nanoparticles and their stability, as well as provide information related to nanoparticle formation and optical properties of nanoparticles based on absorbance values and maximum wavelength. FT-IR analysis was used to identify the functional groups involved in the functional groups involved in the reduction and stabilization of copper ions

during nanoparticle synthesis, which can further provide information on secondary metabolites acting as reducing agents. XRD technique was applied to identify the crystalline phase and analyze the crystal structure of the copper nanoparticles. SEM was employed to examine surface morphology and microstructural features at high resolution, while PSA analysis was performed to determine the particle size distribution of the nanoparticles produced.

2.7. Alpha amylase enzyme inhibition analysis

2.7.1. Maltose standard determination

2.7.1.1. Preparation of 1000 mg/L master solution

Maltose monohydrate 0.01 g was dissolved in distilled water, then put into a 10 mL volumetric flask and diluted to the limit mark, then homogenized.

2.7.1.2. Preparation of Standard Solution

Preparation of standard solution through a dilution process of 1000 mg/L master solution. The preparation of standard solution can be seen in Table 1.

Table 1. Preparation of Maltose Standard Solution

Standard Solution (mg/L)	Volume of Master Solution (mL)	Volume of distilled water (mL)	Total Volume (mL)
80	0.12	1.38	1.50
150	0.225	1.275	1.50
200	0.30	1.20	1.50
300	0.45	1.05	1.50
400	0.60	0.90	1.50
600	0.90	0.60	1.50

2.7.1.3. Maltose standard measurement

Test tubes containing blank solutions, and standard solutions with concentrations of 80; 150; 200; 300; 400; and 600 mg/L with a volume of 1.5 mL were prepared and labeled. Subsequently, 1.5 mL of DNS reagent was added, and the mixture was homogenized using a vortex mixer for 10 s. Then each test tube was placed in a boiling water bath and boiled for 10 minutes. Next, each test tube was put into cold water. Then the absorbance was measured at its maximum absorbance wavelength.

2.7.2. Activity Test

2.7.2.1. Blank

A mixture of 0.5 mL phosphate buffer pH 7.0, 0.5 mL distilled water, and 0.5 mL 2% starch substrate was transferred into a test tube, then incubated at 37°C for 60 minutes. Next, 1.5 mL of DNS reagent was added to the mixture, and was then mixed using a vortex mixer for 10 seconds. Following the mixture was heated in boiling water for 10 minutes, it was cooled in ice water. The absorbance of the reaction was measured at the maximum wavelength.

2.7.2.2. Acarbose (comparator)

A mixture of 0.5 mL of acarbose solution, 0.5 mL of α-amylase enzyme solution, and 0.5 mL of 2% starch substrate was transferred into a test tube, subsequently incubated at 37°C for 60 minutes. Next, 1.5 mL of DNS reagent was added to the mixture, then shaken with a vortex for 10 seconds. Then the mixture was heated in boiling water for 10 minutes, then cooled in ice water. The absorbance of the reaction was measured at the maximum wavelength.

2.7.2.3. α-Amylase enzyme activity (negative control)

A mixture of 0.5 mL of phosphate buffer (pH 7), 0.5 mL of α-amylase enzyme solution, and 0.5 mL of 2% starch substrate was put into a test tube, then incubated at 37°C for 60 minutes. After 1.5 mL of DNS reagent was added to the mixture, it was mixed using a vortex mixer for 10 s. The mixture was further heated in boiling water for 10 minutes and cooled in ice water. The absorbance of the reaction was measured at the maximum absorbance wavelength.

The released maltose was quantified and used to calculate α-amylase activity according to Eq. (1):

$$EA\ (U/mL) = ([Maltosa] \times DF)/(MW \times V \times t) \quad (1)$$

The enzyme activity (EA) was calculated from the maltose concentration produced during the reaction, expressed in parts per million (ppm). This value is then multiplied by the dilution factor (DF) to correct for the dilution effect of the sample. Further, the molecular weight (MW) of maltose is used in the calculations to convert the concentration into number of moles. Meanwhile, the volume of enzyme (V) used, expressed in milliliters, as well as the incubation time (t) in minutes, are also taken into account to quantify the enzyme activity rate.

2.7.2.4. Samples (Binahong leaf extract, CuNPs, and combination of binahong leaf extract + CuNPs)

A mixture of 0.5 mL of samples (with concentrations of 1; 2; 4; 8; and 16 mg/L), each added 0.5 mL of α-amylase enzyme solution, and 0.5 mL of 2% starch substrate was added to a test tube. It was then incubated at 37°C for 60 minutes. After 1.5 mL of DNS reagent was added to each mixture, it was mixed using a vortex mixer for 10 s. The mixture was further heated in boiling water for 10 minutes, then cooled in ice water. The absorbance of the reaction was measured at the maximum absorbance wavelength and the Relative Activity (RA) percent was calculated using equation (2) and the Inhibition percent using equation (3).

$$RA = \frac{\text{Inhibitory Activity}}{\text{Activity Without Inhibiting Substance}} \times 100\% \quad (2)$$

$$\%\ \text{Inhibition} = 100 - \%\ \text{Relative Activity} \quad (3)$$

IC_{50} represents the concentration of an inhibitor that causes 50% inhibition of α-amylase activity. The IC_{50} value is calculated using a linear regression equation, where the inhibitor concentration and percentage inhibition were used as the x- and y-axes, respectively. Based on the linear regression equation y = ax + b, the IC_{50} was calculated using equation (4):

$$IC_{50} = \frac{50-b}{a} \quad (4)$$

In a linear regression equation, the parameter a represents the slope, indicating the rate of change, which represents the rate of change of the dependent variable with respect to the independent variable. The parameter b corresponds to the intercept, which is the value at which the regression line intersects the y-axis.

3. Results and Discussion

3.1. Phytochemical test

Phytochemical analysis of Binahong leaf extract used in this study showed the presence of flavonoid and saponin compounds. This result differs from previous findings reported by Munandar et al. [14], which is the presence of flavonoids, saponins, and tannins in similar extracts. This discrepancy is most likely attributed to geographical variation in the plant source, given that the samples in this study were obtained from the Manado region of North Sulawesi, Indonesia. The phytochemical analysis was conducted to identify secondary metabolites with potential reducing activity in copper nanoparticle biosynthesis. The complete phytochemical results are presented in Table 2.

Table 2. Phytochemical Analysis

Phytochemical Test	Result
Alkaloids	-
Flavonoids	+
Saponins	+
Steroids	-
Tannins	-
Terpenoids	-

3.2. Optimization of CuNPs by pH Determination

pH optimization indicates that CuNP formation is strongly governed by the reaction medium, as evidenced by increased intensity and band sharpness in the UV–Vis spectra (Fig. 1). Under more alkaline conditions, a higher fraction of deprotonated phenolic/flavonoid functional groups is present, which enhances the reduction of Cu^{2+} and improves particle stabilization; consequently, the CuNP absorption band becomes more distinct and intense.

This trend is consistent with previous reports indicating that plant-extract–mediated CuNP synthesis commonly exhibits an optimum in the neutral-to-alkaline range, for example at pH 9 [15] and pH 10 [16], which is typically indicated by the strongest UV–Vis response compared with other pH conditions.

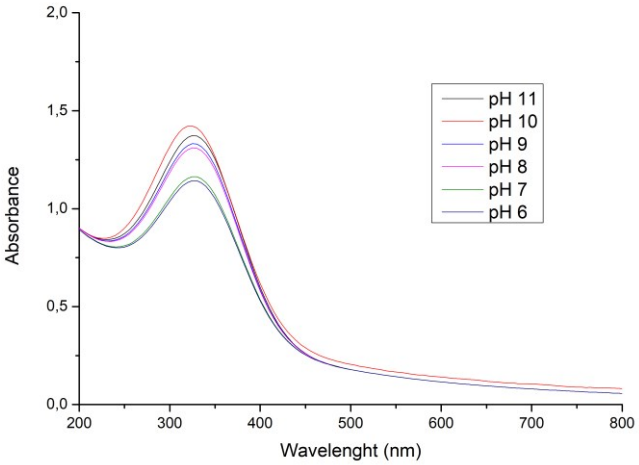

Fig. 1. UV-Vis spectra of CuNPs at varying pH values

The slight decrease in peak intensity at pH 11 relative to pH 10 can be attributed to changes in solution chemistry at highly alkaline pH; excessive alkalinity can shift Cu^{2+} speciation toward hydroxide species (e.g., $Cu(OH)_2$) and promote particle growth/aggregation, leading to a less optimal spectral response even though nanoparticles may still form [17]. Other systems also report different optima (e.g., pH 9) depending on the plant extract and reaction conditions, confirming that the "optimum pH" is system-specific [15]. Importantly, a strong band around 325 nm is also frequently reported for CuO/Cu_2O nanoparticles; therefore, If the intended target is metallic Cu^0, the presence of a strong band around 325 nm may indicate the presence of an oxide shell or $CuO–Cu_2O$ products, and confirmation by XRD and FTIR is therefore recommended to verify the dominant phase [18].

3.3. Synthesis of Cu nanoparticles

Nanoparticle synthesis on a scaled-up synthesis was carried out to obtain nanoparticle powder in large quantities. Nanoparticle synthesis was carried out in a ratio of 1:3 (Binahong extract: Cu^{2+} precursor solution). The visual appearance of nanoparticle synthesis are shown in Fig. 2.

The color change of the synthesized copper nanoparticles is shown in Fig. 2, where the solution turns from brown to green in a span of about three hours, indicating the formation and partial oxidation of CuNPs to copper oxide. This color change phenomenon is in line with the report of Zambare et al. [19] on the synthesis of CuNPs using *Ocimum sanctum* extract, who noted a color shift from blue to green within 30-60 minutes as an early indicator of nanoparticle formation through the reduction of Cu^{2+} by phytochemical compounds such as polyphenols and terpenoids. Similar mechanisms have been reported in recent studies, where the color change from brown to green suggests partial conversion of Cu^0 to CuO, which also affects the optical properties, particularly the SPR-related absorption band in the UV–Vis spectrum [20,21]. Therefore, the color change in Fig. 2 is not only a marker of the formation of CuNPs, but also an early signal of oxidation

of the nanoparticle surface, which should be carefully controlled to maintain the stability and integrity of the particles.

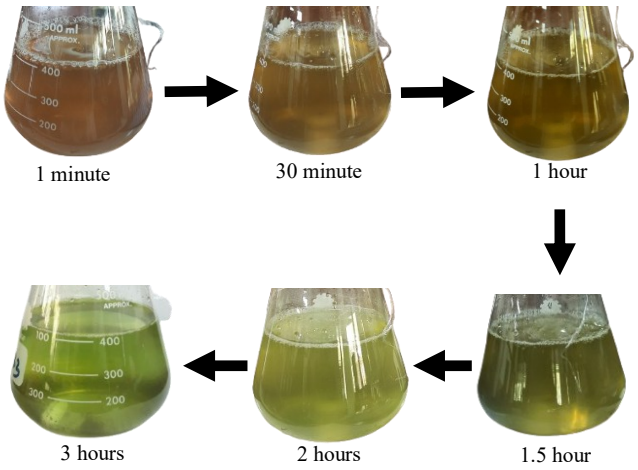

Fig. 2. Synthesis result of Cu nanoparticles

3.4. UV-Vis spectroscopy analysis results

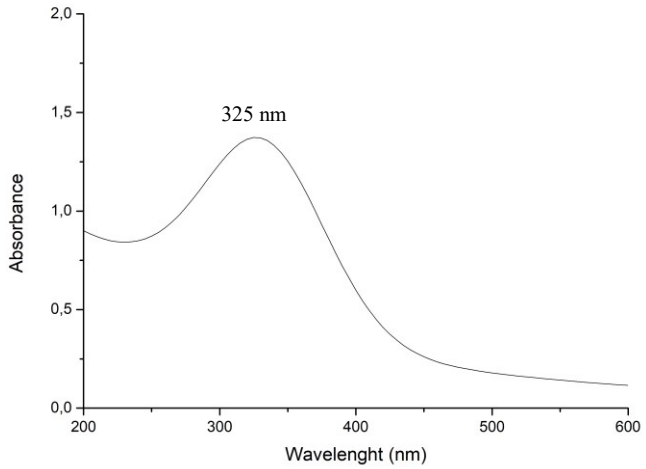

Fig. 3. UV-Vis spectra Cu nanoparticle

The UV–Vis spectrum as shown in Fig. 3 exhibits a strong, broad absorption band around 325 nm, followed by a sharp decrease around 400 nm and weak absorption continuing up to 600 nm. Such behavior is commonly attributed to formation of oxide-based copper nanostructures (CuO/Cu_2O) or copper that rapidly oxidizes/develops an oxide shell, because dominant UV absorption is often associated with charge-transfer or band-to-band transitions in Cu–O bonding. Furthermore, the typical feature of pure metallic Cu^0 in the visible region is often suppressed due to surface oxidation and/or particle polydispersity. The broad absorption band indicates polydispersity and the presence of an organic capping layer, leading to band broadening and baseline elevation due to light scattering and aggregation. Similar UV–Vis features have been reported for other metal nanoparticles, such as AgNPs, where capping variations induce spectral shifts [22]. In addition, comparable UV–Vis behavior has been reported for AgNPs and CuO/Cu_2O nanostructures [23], the observed spectrum can be regarded as an optical fingerprint of Cu–O nanophase formation.

3.5. XRD pattern of CuNPs synthesized using A. cordifolia

The XRD diffractogram of the CuNps sample as shown in the Fig. 4 reveals several characteristic peaks indicating cuprous oxide (Cu_2O) as the dominant component, evidenced by characteristic reflections at 2θ = 29.6° (110), 36.4° (111), 42.3° (200), 61.3° (220), 73.5° (311), and 77.3° (222). These peaks are commonly reported as reference peaks for Cu_2O identification in copper-based systems [24,25]. On the other hand, the peaks/components near 43.3°, 50.4°, and 74.1° may be attributed to fcc metallic copper (Cu^0) and/or peak overlap with adjacent Cu_2O reflections, since these angles are common signatures of Cu^0 [26]. If CuO were formed in a significant amount, additional characteristic peaks would typically appear around 32.5°, 35.5°, 38.7°, 48.8°, 53–58°, 61.5°, and 66°; because their absence indicates that CuO is not the dominant crystalline phase [27].

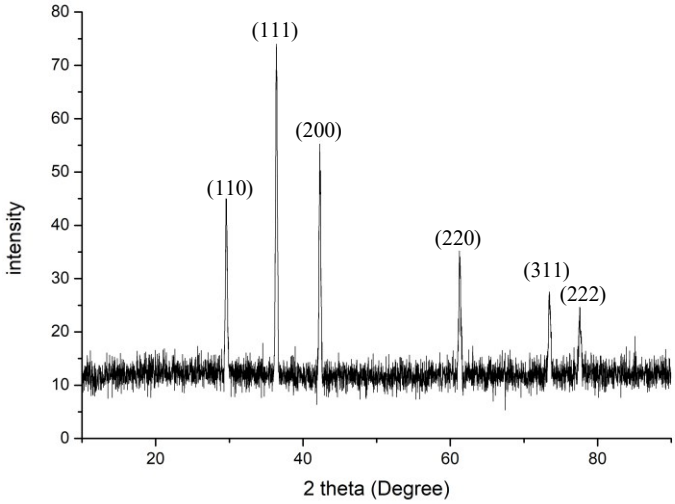

Fig. 4. Diffractogram of Copper nanoparticles

Overall, the observed peak pattern suggests that the synthesized product is more likely composed of Cu_2O nanocrystals as the dominant phase, with a minor residual contribution from Cu^0 and/or peak overlap in certain reflections, while CuO does not appear to be the primary crystalline phase. Such a phase composition is common in reduction-based syntheses (including green synthesis), as Cu^0 can undergo partial oxidation to Cu_2O during the reaction, separation, drying, or exposure to air, thereby resulting in XRD patterns dominated by the thermodynamically more stable oxide phase.

3.6. Functional group identification by FTIR analysis

The Fourier Transform Infrared (FTIR) spectrum of the copper nanoparticle sample shows characteristic spectral features indicating that the synthesis was carried out via a plant-mediated green synthesis route, consistent with recent reports on plant-mediated nanoparticle synthesis. This spectrum is dominated by two major categories of absorption bands, originating from organic biomolecules and metal–oxide (Cu–O) bonds.

As shwon in Fig. 5. the FTIR spectrum exhibits a broad absorption band at 3200–3600 cm^{-1}, attributable to O–H stretching (hydroxyl groups) and absorption bands at 2920–2850 cm^{-1} corresponding to aliphatic C–H stretching, suggesting the presence of residual organic species and/or adsorbed surface water serving as stabilizing components. Comparable FTIR features for green-synthesized Cu_2O have been reported by Abdelbaki et al. [28], where O–H and C–H bands appear together with Cu–O bands, suggesting the involvement of plant-extract biomolecules in reduction and capping. A strong band near 1600 cm^{-1}, commonly assigned to C=O (amide I) and/or aromatic C=C vibrations, along with bands near 1400 cm^{-1} and 1000–1100 cm^{-1} (vibrations of COO^-/C–O/C–O–C), further corroborates the presence of organic ligands (e.g., phenolic, carbonyl, or polysaccharide groups) coordinated to the particle surface, thereby enhancing colloidal stability.

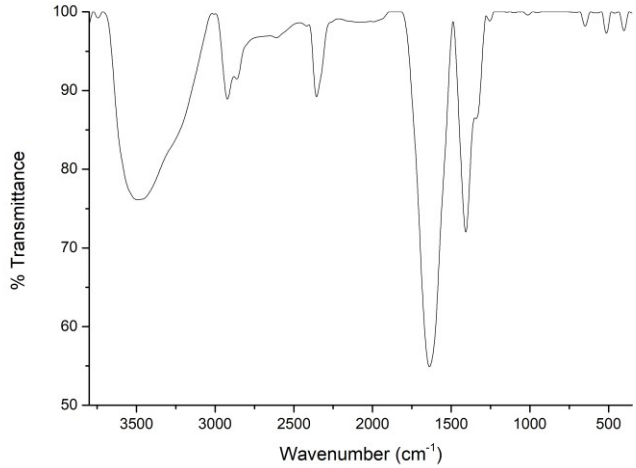

Fig. 5. FTIR Spectrum of CuNPs synthesized by *A. cordifolia*

This pattern of organic-related bands is consistent with previous discussions on surface functional groups of Cu_2O/CuO nanoparticles in the comparative study by Havryliuk et al. [18]. The most diagnostic feature of Cu_2O is the low-wavenumber band at 600–620 cm^{-1}, corresponding to Cu–O (Cu(I)–O) vibrations. This band position is commonly used to confirm Cu_2O formation and to distinguish it from CuO, whereas CuO typically exhibits Cu–O bands at lower wavenumbers or with different spectral components [18] and as also reported for Cu_2O-based composite systems retaining the characteristic Cu–O band of Cu_2O [29].

3.7. SEM of CuNPs synthesized by A. cordifolia

As shown in Fig. 6, a morphology of quasi-spherical granules was observed in SEM image. Those are not individually dispersed, forming micrometer-sized aggregates/clusters distributed over a relatively rough/porous surface matrix. Visually, the apparent primary granules are in the sub-micrometer range, whereas the secondary aggregates can reach several micrometers. This pattern is common for wet-chemical or biogenic Cu and copper-oxide materials because their high surface energy promotes interparticle (van der Waals) attraction and agglomeration during drying. The aggregation tendency of green-synthesized CuO/Cu_2O is commonly attributed to interactions among particles and viscous extract components, as well as residual organic species acting as interparticle bridging agents, resulting in asymmetric clusters and an organic-rich surface layer [17,30].

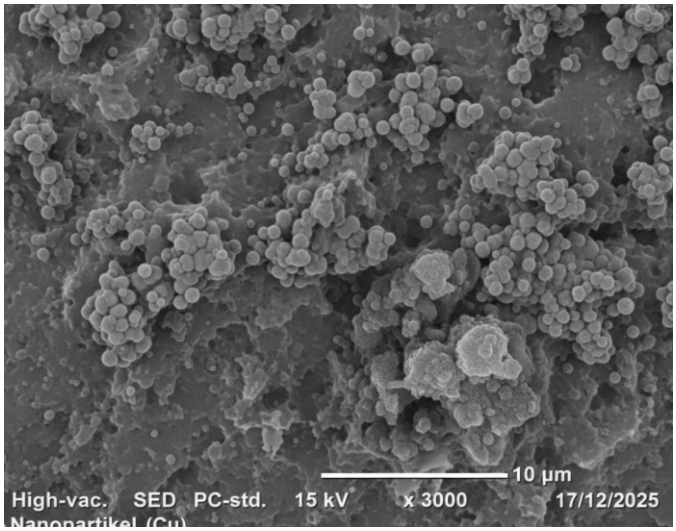

Fig. 6. (SEM morphological analysis of CuNPs

Previous comparative studies suggest that phytochemical capping is sufficiently strong and the surface charge is adequate, particles tend to exhibit improved monodispersity with minimal agglomeration; conversely, insufficient capping combined with high aggregation leads to SEM morphologies dominated by clustered structures [31]. Synthesis parameters such as pH, temperature, precursor concentration, and extract dosage are known to shift the particle size and degree of agglomeration in CuO/Cu_2O, rendering the observed aggregation pattern consistent with the applied reaction conditions and post-synthesis processing [32].

3.8. Distribution of Cu nanoparticle particle sizes using PSA

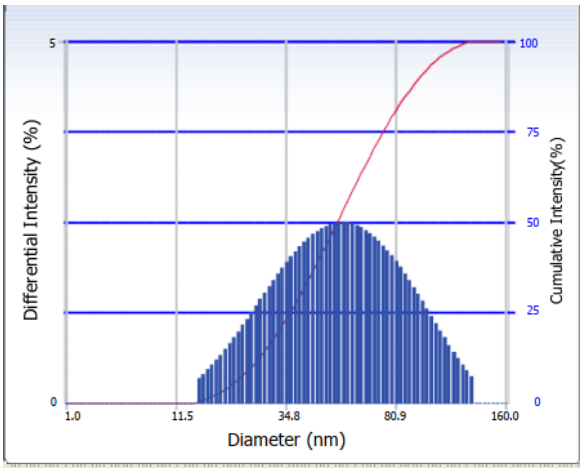

Fig. 7. CuNps Intensity Distribution

Fig. 7 presents the particle size distribution of Cu nanoparticles as determined by PSA with a diameter range of approximately 10 to 150 nm. The blue curve corresponds to the differential intensity distribution (%), while the red curve shows the cumulative intensity (%). Based on the distribution

peak, the most dominant particle size is in the range of 60–70 nm, indicating that most particles are smaller than 100 nm and thus confirming their classification within the nanoscale regime.

The cumulative intensity value reaches 100% at a size of around 150 nm, which means that there are no particles larger than this limit. This narrow distribution suggests favorable colloidal stability, as small particles tend to have sufficient electrostatic repulsive forces to prevent agglomeration.

Overall, these PSA results show that the Cu nanoparticles formed have a dominant size in the range of 60–70 nm, a narrow size distribution, and good dispersion stability, indicating the success of the synthesis process in producing nanoparticles with nanoscopic sizes and low agglomeration levels. From the curve, the average size of the nanoparticles is obtained an average hydrodynamic diameter of approximately 65 nm.

When compared with recent literature, the resulting particle size can be regarded as competitive for Cu-based nanoparticles produced via green synthesis. For example, in CuO-NPs, Saha et al. (2023) [33] reported that the DLS size was larger than the FESEM size (approximately 117 nm vs 98 nm) due to dispersion and surface-related effects in suspension, while Shafiq et al. (2024) [34] showed an even more pronounced discrepancy (TEM 11 nm but DLS 273 nm), attributed to particle agglomeration during aqueous DLS measurements.

3.9. α-Amylase enzyme inhibition test

Table 3. Percentage inhibition value and IC_{50} of samples

Sample	Concentration (μg/mL)	Inhibition (%)	IC_{50} (μg/mL)
Acarbose	1	24.72	5.04
	2	33.71	
	4	49.43	
	8	70.78	
	16	99.43	
A. cordifolia extract	1	7.86	8.89
	2	17.41	
	4	28.65	
	8	51.12	
	16	80.89	
CuNPs	1	21.35	6.18
	2	30.33	
	4	42.69	
	8	59.55	
	16	96.62	
A. cordifolia extract + CuNPs	1	15.17	6.83
	2	25.84	
	4	38.20	
	8	60.11	
	16	94.38	

Based on α-amylase inhibition assay, all samples exhibit a dose-dependent response, and the inhibitory potency ranked by IC_{50} values follows: acarbose (5.04 μg/mL) > CuNPs (6.18 μg/mL) > extract + CuNPs (6.83 μg/mL) > A. cordifolia extract (8.89 μg/mL). This confirms that CuNPs inhibit starch hydrolysis with efficacy comparable to the drug control, suggesting potential to reduce postprandial glucose spikes (the same therapeutic target addressed by α-amylase inhibitors such as acarbose). Mechanistically, inhibition by Cu/Cu-oxide–based nanoparticles is commonly attributed to nanoparticle–enzyme surface adsorption and interaction mechanisms (including electrostatic interactions, hydrogen bonding, and other surface contacts) that can hinder substrate access or induce conformational changes in the enzyme, with an additional contribution from dissolved Cu ionic species interacting with functional amino acid residues. Concentration-dependent α-amylase inhibition by CuO/Cu-based nanoparticles has been widely reported in recent in vitro studies [35-37].

The observation that the extract+CuNPs combination does not exhibit higher inhibitory potency than CuNPs alone, can be explained by extract components forming a thicker organic capping layer that masks active surface sites and/or alters dispersion (aggregation), thereby reducing the effective surface area available to interact with the enzyme. This capping-related effect is frequently highlighted in reviews of CuO nanoparticles for biomedical/nanomedicine applications [38] and in green-synthesis systems highlighting the role of phytochemicals as reducing agents, stabilizers, and capping agents [14].

4. Conclusion

This study demonstrates that green synthesis using Binahong (*Anredera cordifolia*) leaf extract can produce copper-based nanomaterials dominated by the Cu_2O phase and stabilized by plant-derived biomolecules. The in vitro results show that the CuNPs exhibit pronounced α-amylase inhibitory activity that increases in a concentration-dependent manner, with potency approaching that of acarbose. These findings indicate that Cu_2O nanoparticles obtained via green synthesis show promise as an early-stage antidiabetic candidate for postprandial glucose control, particularly for screening and formulation development. However, several limitations should be acknowledged. First, the antidiabetic evaluation was limited to an in vitro α-amylase assay, so the biological efficacy cannot yet be extrapolated to in vivo systems. Second, the morphological data indicate a tendency toward particle aggregation, which may affect colloidal stability and the consistency of bioactivity; therefore, further optimization of dispersion and stability (e.g., zeta potential and PDI) is therefore required. Third, the possible contribution of minor phases (e.g., Cu^0/other oxides) and the influence of residual organic capping on the inhibition mechanism were not quantitatively distinguished. Accordingly, future work should include enzyme-inhibition kinetics (to determine the inhibition type), additional target enzymes (e.g., α-glucosidase), safety/biocompatibility testing, and in vivo efficacy validation to comprehensively assess the translational potential of these nanoparticles as antidiabetic candidates.

Acknowledgements

The author would like to thank DIPA Universitas Sam Ratulangi for its support and funding for this research, that enabled the successful completion of this research.

References

1. N.H. Cho, J.E. Shaw, S. Karuranga, Y. Huang, J.D. da Rocha Fernandes, A.W. Ohlrogge, B. Malanda, *IDF Diabetes Atlas: Global estimates of diabetes prevalence for 2017 and projections for 2045*, Diabetes Res. Clin. Pract. 138 (2018) 271–281.
2. C.C. Patterson, S. Karuranga, P. Salpea, P. Saeedi, G. Dahlquist, G. Soltesz, G.D. Ogle, *Worldwide estimates of incidence, prevalence and mortality of type 1 diabetes in children and adolescents: Results from the International Diabetes Federation Diabetes Atlas, 9th edition*, Diabetes Res. Clin. Pract. 157 (2019) 107842.
3. D.S. Prawitasari, *Diabetes Melitus dan Antioksidan*, Keluwih: Jurnal Kesehatan dan Kedokteran 1 (2019) 47–51.
4. C.A. Pieme, J.A. Tatangmo, G. Simo, P.C. Biapa Nya, V.J. Ama Moor, B. Moukette Moukette, F. Tankeu Nzufo, B.L. Njinkio Nono, E. Sobngwi, *Relationship between hyperglycemia, antioxidant capacity and some enzymatic and non-enzymatic antioxidants in African patients with type 2 diabetes*, BMC Res. Notes 10 (2017) 141.
5. A.B. Oyenihi, A.O. Ayeleso, E. Mukwevho, B. Masola, *Antioxidant strategies in the management of diabetic neuropathy*, BioMed Res. Int. 2015 (2015) 515042.
6. Erlidawati, S. Safrida, M. Mukhlis, *Potensi Antioksidan Sebagai Antidiabetes: Buku untuk mahasiswa*, Syiah Kuala University Press (2018) 1–130.
7. R. Kitture, K. Chordiya, S. Gaware, S. Ghosh, P.A. More, P. Kulkarni, B.A. Chopade, S.N. Kale, *ZnO nanoparticles-red sandalwood conjugate: a promising anti-diabetic agent*, J. Nanosci. Nanotechnol. 15 (2015) 4046–4051.
8. A.B. Patil, S. Ghosh, S.D. Phadatare, P. Pathak, G.K. Sharma, B.A. Chopade, V.S. Shinde, *Evaluation of malonic acid diamide analogues as radical scavenging agents*, New J. Chem. 39 (2015) 1267–1273.
9. V.P. Roseline, V. Priya, *Antidiabetic potential of copper oxide nanoparticles using biological and polymer functionalized method mediated by Sarcostemma acidum stem extract*, Orient. J. Chem. 39 (2023) 387–392.
10. S. Ghosh, P. More, R. Nitnavare, S. Jagtap, R. Chippalkatti, A. Derle, R. Kitture, A. Asok, S. Kale, S. Singh, M.L. Shaikh, B. Ramanamurthy, J. Bellare, B.A. Chopade, *Antidiabetic and antioxidant properties of copper nanoparticles synthesized by medicinal plant Dioscorea bulbifera*, J. Nanomed. Nanotechnol. S6 (2015) 007.
11. R. Singh, L.U. Nawale, M. Arkile, U.U. Shedbalkar, S.A. Wadhwani, D. Sarkar, B.A. Chopade, *Chemical and biological metal nanoparticles as antimycobacterial agents: A comparative study*, Int. J. Antimicrob. Agents 46 (2015) 183–188.
12. F. Buazar, S. Sweidi, M. Badri, F. Kroushawi, *Biofabrication of highly pure copper oxide nanoparticles using wheat seed extract and their catalytic activity: A mechanistic approach*, Green Process. Synth. 8 (2019) 691–702.
13. S.C. Wattimena, P.J. Patty, *Antibacterial properties of silver nanoparticles synthesized using leaf extract of Anredera cordifolia as a reducing agent*, World J. Pharm. Pharm. Sci. 6 (2017) 1673–1683.
14. N. Munandar, S. Kasim, R. Arfah, D.N. Basir, Y. Hala, M. Zakir, H. Natsir, *Green synthesis of copper oxide (CuO) nanoparticles using Anredera cordifolia leaf extract and their antioxidant activity*, Commun. Sci. Technol. 7 (2022) 127–134.
15. A.A. Disher, A.M.A. Al-Kufaishi, Z.M. Najm, A.A.M. Mohammed, L.A.M. AlMashhedy, B.M. Alshelah, B.H. Al-Kinani, *Ecofriendly synthesis of copper nanoparticles using coriander seeds for enhanced adsorption efficiency*, Open Biotechnol. J. 19 (2025) e18740707373773.
16. R.W.H. Putri, S. Sutoyo, *The potency of noni leaves extract (Morinda citrifolia L.) as a bioreductor in the synthesis of copper nanoparticles and its effectiveness as an antibacterial against Streptococcus pyogenes*, Jurnal Kimia Sains dan Aplikasi 28 (2025) 138–145.
17. M.B. Mobarak, M.F. Sikder, K.S. Muntaha, S. Islam, S.M.F. Rabbi, F. Chowdhury, *Plant extract-mediated green-synthesized CuO nanoparticles for environmental and microbial remediation: A review covering basic understandings to mechanistic study*, Nanoscale Adv. 7 (2025) 2418–2445.
18. O. Havryliuk, G. Rathee, J. Blair, V. Hovorukha, O. Tashyrev, J. Morató, L.M. Pérez, T. Tzanov, *Unveiling the potential of CuO and Cu_2O nanoparticles against novel copper-resistant Pseudomonas strains: An in-depth comparison*, Nanomaterials 14 (2024) 1644.
19. P. Zambare, A. Survase, S. Kanase, Green synthesis of copper nanoparticles using leaf extract of Ocimum sanctum and its antimicrobial activity, Int. J. Pharm. Investig. 13 (2023) 106–112.
20. A. Nazir, S. Aslam, P. Akhter, O.A. Mohammed, A.S. Doghish, N. Alwadai, A. Ali, H. Arif, M. Iqbal, *Effect of iron doping on titania nanoparticles derived from Dalbergia sissoo for removal of tetracycline hydrochloride*, Semiconductors 59 (2025) 291–299..
21. B. Ahmed, M.B. Tahir, M. Sagir, M. Hassan, *Bio-inspired sustainable synthesis of silver nanoparticles as next generation of nanoproduct in antimicrobial and catalytic applications*, Mater. Sci. Eng. B 301 (2024) 117165.
22. T.D. Nguyen, T.P.-N. Nguyen, N.T.-T. Thai, Y.H. Hoang, G.T.-N. Trinh, *Investigating the antimicrobial activity of silver nanoparticles with varying charges green-synthesized from Tabebuia rosea flower*, Commun. Sci. Technol. 9 (2024) 398–410.
23. S. Sujinnapram, K. Kengtone, C. Raktham, K. Hongsith, S. Choopun, S. Wongrerkdee, *Tunable copper oxide quantum dots: electrochemical synthesis, characterization, and advanced applications*, Commun. Sci. Technol. 10 (2025) 45–51.
24. C.-J. Chang, C.-W. Kang, A. Pundi, *Effect of calcination-induced oxidation on the photocatalytic H_2 production performance of cubic Cu_2O/CuO composite photocatalysts*, Catalysts 14 (2024) 926.
25. X. Luo, C. Zhou, H. Teng, X. Li, H. Tian, X. Ji, C. Liu, *Hexagonal dendritic Cu_2O: a breakthrough in photocatalytic efficiency for CR dye degradation*, Chem. Phys. Lett. 876 (2025) 142293.
26. D. Papamichail, F. Franceschini, I. Abbas, D. Balalta, T.T.H. Nguyen, D. Pant, S. Bals, I. Taurino, E. Janssens, D. Grandjean, P. Lievens, *Nanostructuring copper thin film electrodes for CO_2 electroreduction to C_{2+} products*, Nanoscale 17 (2025) 17745–17757.
27. S. Feng, X. Xing, W. Hou, *Copper oxide nanoparticles modified electrodes for high-sensitivity detection of uric acid in athletes*, Alex. Eng. J. 101 (2024) 1–7.
28. H. Abdelbaki, A. Djemoui, L. Souli, A. Souadia, M.R. Ouahrani, B. Djemoui, M.B. Lahrech, M. Messaoudi, I. Ben Amor, A. Benarfa, A. Alsalme, M. Bechelany, A. Barhoum, *Plant mediated synthesis of flower-like Cu_2O microbeads from Artimisia campestris L. extract for the catalyzed synthesis of 1,4-disubstituted 1,2,3-triazole derivatives*, Front. Chem. 11 (2024) 1342988.
29. Y. Li, M. Yan, X. Li, J. Ma, *Construction of Cu_2O-ZnO/Cellulose composites for enhancing the photocatalytic performance*, Catalysts 14 (2024) 476.
30. J. Neiva, Z. Benzarti, S. Carvalho, S. Devesa, *Green synthesis of CuO nanoparticles—structural, morphological, and dielectric characterization*, Materials 17 (2024) 5709.
31. M. Salama, P.C. Pwavodi, *Green synthesis of CuO nanoparticles from Punica granatum leaves and their application in the enhancement of cold-pressed calcareous alkali-activated materials for sustainability*, PLOS ONE 20 (2025) e0336812.

32. B. Djamila, L.S. Eddine, B. Abderrhmane, N. Allag, A. Barhoum, *In vitro antioxidant activities of copper mixed oxide (CuO/Cu₂O) nanoparticles produced from the leaves of Phoenix dactylifera L.*, Biomass Conv. Bioref. 14 (2024) 6567–6580.
33. T. Saha, M.B. Mobarak, M.N. Uddin, M.S. Quddus, M.R. Naim, N.S. Pinky, *Biogenic synthesis of copper oxide (CuO) NPs exploiting Averrhoa carambola leaf extract and its potential antibacterial activity*, Mater. Chem. Phys. 305 (2023) 127979.
34. A. Shafiq, U. Jeong, Y. Han, Y. Kim, J. Lee, B.S. Kim, *Green Synthesis of Copper Oxide Nanoparticles from Waste Solar Panels Using Piper nigrum Fruit Extract and Their Antibacterial Activity*, Catalysts 14 (2024) 472.
35. K. Ramasubbu, S. Padmanabhan, K.A. Al-Ghanim, M. Nicoletti, M. Govindarajan, N. Sachivkina, V.D. Rajeswari, *Green Synthesis of Copper Oxide Nanoparticles Using Sesbania grandiflora Leaf Extract and Their Evaluation of Anti-Diabetic, Cytotoxic, Anti-Microbial, and Anti-Inflammatory Properties in an In-Vitro Approach*, Fermentation 9 (2023) 332.
36. A. Relhan, S. Guleria, A. Bhasin, A. Mirza, J.L. Zhou, *Biosynthesized copper oxide nanoparticles by Psidium guajava plants with antibacterial, antidiabetic, antioxidant, and photocatalytic capacity*, Biomass Conv. Bioref. 15 (2025) 26623–26640.
37. R. Shanmugam, T. Munusamy, A.M. Nisha, A. Rajaselin, S. Govindharaj, *Exploring the In Vitro Antidiabetic Potential of Metal Oxide Nanoparticles Synthesized Using Lemongrass and Mint Formulation*, Cureus 16 (2024) e53489.
38. M. Devaraji, P.V. Thanikachalam, K. Elumalai, *The potential of copper oxide nanoparticles in nanomedicine: A comprehensive review*, Biotechnol. Notes 5 (2024) 80–99.